AJP

ISSN : 0971 - 3093

Vol 34, Nos 3 & 4, March-April, 2025

ASIAN JOURNAL OF PHYSICS

An International Peer Reviewed Research Journal

P K Kaw Memorial Issue

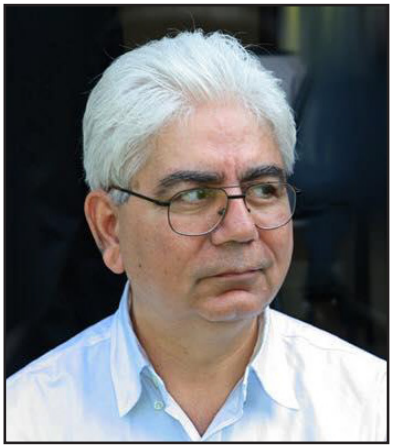

Prof P K Kaw

Guest Editors : Ramesh Narayanan & Satyananda Kar

ap

ANITA PUBLICATIONS

FF-43, 1st Floor, Mangal Bazar, Laxmi Nagar, Delhi-110 092, India

B O : 2, Pasha Court, Williamsville, New York-14221-1776, USA

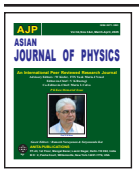

Asian Journal of Physics
Vol. 34, Nos 3 & 4 (2025) 187-200
Available on: www.asianjournalofphysics.com

ap

Study of compact electron cyclotron resonance plasma thruster under various conditions

N Balachandran, D Sahu, R Narayanan, and A Ganguli
Department of Energy Science and Engineering,
Indian Institute of Technology Delhi, Hauz Khas, New Delhi-110 016, India

Dedicated to Prof P K Kaw

Plasma thrusters for deep space plasma propulsion has been gaining impetus in the recent past. Some of the major R & D work has been on Hall thrusters, rf based helicon thrusters, VASIMIR, etc., which are either dc/pulsed DC or rf based. These plasma thrusters are a significant part of the altitude and orbit control system of a spacecraft that is used for various scientific missions and communication purposes. Although the thrust levels may be only a few mN, the specific impulse obtained can be very high. However, very few efforts have been undertaken using electron cyclotron resonance (ECR) sources. Plasma Lab at IIT Delhi has recently shown the efficacy of an indigenously developed Compact ECR Plasma Source (CEPS) to be used as a plasma thruster. CEPS is a microwave (2.45 GHz) energized plasma source developed at the Plasma Lab, IIT Delhi. Various experimental as well as theoretical studies have been done on the CEPS establishing it as an efficient plasma source suitable for various industrial applications. In this work, a finite element software, COMSOL Multi-physics, was used to simulate the Argon plasma dynamics, under different operating conditions, in a CEPS thruster that was attached to an expansion chamber. The study was conducted in two phases, starting with the simulation of a stationary magnetic field using permanent ring magnets from the CEPS in Phase I. This field data was then implemented for the ECR microwave plasma simulation in phase II. The initial findings of the plasma parameters, under different operating conditions, are compared with the experimental results and verified.

doi: 10.54955/AJP.34.3-4.2025.187-200

Keywords: Plasma, Simulation, COMSOL, Argon plasma, ECR, CEPS, Langmuir Probe.

1 Introduction

Electric propulsion (EP) is a class of deep space propulsion devices that are based on different technologies to produce thrust using electric or magnetic field [1]. There are various types of such thrusters [2] developed so far that have their advantages as well as limitations [3]. EP systems differ from other propulsion devices in the method of accelerating the propellant, yet they all share the fundamental objective of converting the stored energy in some form of fuel (solid / liquid / gas) into kinetic energy of the propellant particles. One of the significant issues faced by the EP systems is electrode degradation. Over time, the conductive surfaces that interface with the plasma undergo erosion through sputtering. This erosion is one of the primary drawbacks of traditional EP systems, as it can lead to various performance and longevity issues of the system. An indigenously developed Compact Electron Cyclotron Resonance Plasma Source (CEPS) at the Plasma Lab, IIT Delhi [4-9] has been recently identified as a potential electrodeless thruster which addresses this primary drawback of conventional thrusters, thereby potentially offering improved reliability and longer operational lifetimes. This inference is based on the various studies that have been conducted on

Corresponding authors
e mail: dpsahu@dese.iitd.ac.in (*Debaprasad Sahu*); *rams@dese.iitd.ac.in* (*Ramesh Narayanan*)

CEPS to understand its plasma dynamics including experimental characterization in small, medium and large expansion chambers as well as a theoretical global model to estimate thrust. However, none of the studies have employed simulation tools like COMSOL Multiphysics which can integrate magnetic field, plasma chemistry and microwave power deposition into plasma. The aim of present work is to use the COMSOL Multiphysics software to simulate a CEPS plasma model and to validate the experimental findings.

The structure of the paper is as follows: Section 2 describes the experimental setup, Section 3 outlines the COMSOL model, including the governing equations and reaction modelled, Section 4 presents the key results and discussions, and Section 5 provides a summary of the paper.

2 Experimental Setup

2.1 Compact ECR Plasma Source – CEPS

CEPS is a standalone system including a microwave launcher, impedance matching section, mode converter and a Plasma Source Section (PSS). The microwave launcher is a standard magnetron (2M107-A National: 2.45 GHz, CW-mode operation) coupled to a rectangular waveguide (WR340) to excite a TE10 mode. A transition from a rectangular to a circular waveguide (i.e. transition from a TE10 mode to TE11 mode) is placed in the waveguide line after which the microwave is coupled into the cylindrical vacuum PSS through a quartz window. The microwave coupling into the CEPS is undertaken through electron cyclotron resonance (ECR) mechanism [4-9]. A set of NdFeB ring magnets provides the necessary magnetic fields to form an ECR zone within the PSS of the CEPS, wherein the microwave power is coupled to a cohort of resonating electrons (ECR mechanism), resulting in plasma production inside the PSS. A triple stub tuner is placed in the waveguide line (air side) between the magnetron and the mode-transition waveguide, allowing for dynamic impedance matching the nonlinear plasma load to the magnetron. A schematic of the CEPS is given in Fig 1. The CEPS measures 60 cm in length and weighs 14 kg. A dual directional coupler (Model No.: MM1002C), placed between the magnetron and triple stub-tuner, was used to measure the forward and reflected power in this set of experiments.

(a)

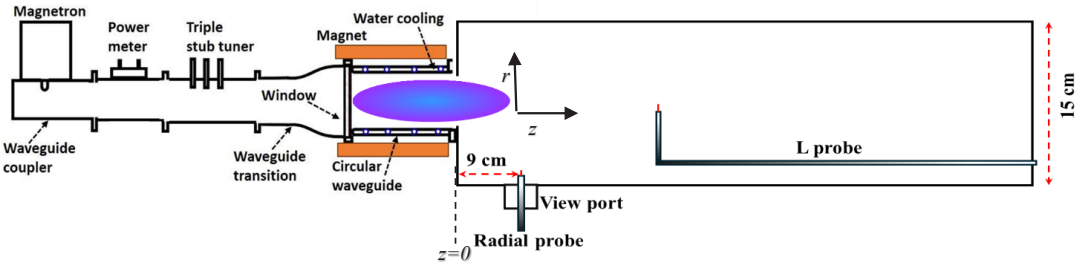

Fig 1. (a). Photo of the setup, (b) Schematics of the setup.

A circulator (Thomson CSF F10573) has also been installed between the magnetron and triple stub-tuner, was used to measure the forward and reflected power in these set of experiments. A circulator (Thomson CSF F10573) has also been installed between the magnetron and dual-directional coupler (DDC). The circulator is installed so as to protect the magnetron from any reflected power, due to an impedance mismatch in the dynamic nonlinear plasma load.

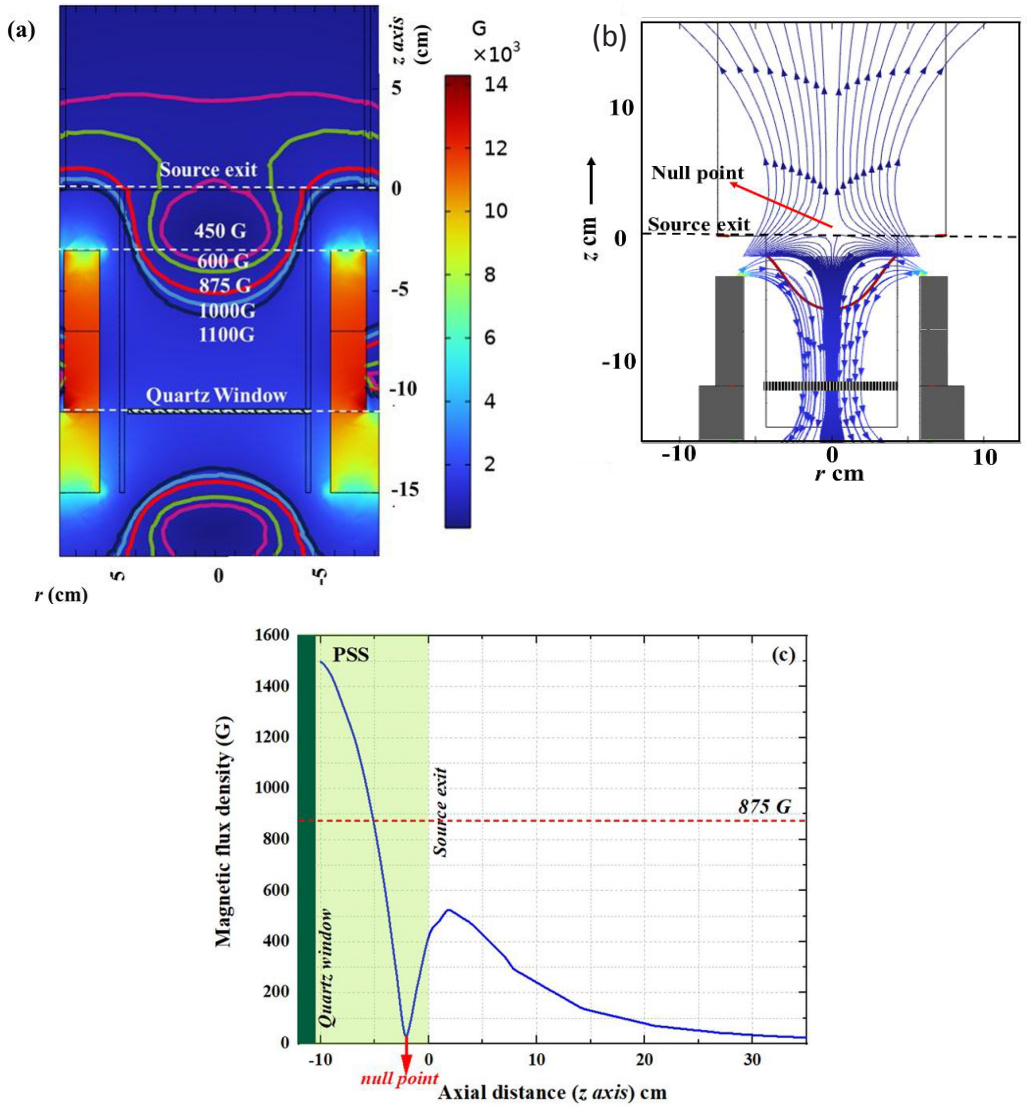

Fig 2. (a) Simulated magnetic field contours and surface plot, (b) Magnetic streamline, (c) Magnetic flux density.

The CEPS magnetic field is produced by a set of coaxial NdFeB ring magnets. The detailed magnetic field configuration is illustrated in the simulation results of Fig 2. An 875 G contour located within the PSS represents the electron cyclotron resonance zone, facilitating plasma production. A characteristic feature of this magnetic field configuration is that the plane containing the magnetic null situated near the source exit demarcates the PSS from the expansion chamber into two distinctly well-defined volumes (Fig 2b). In Fig 2, one observes that the magnetic field lines depict distinctly different characteristic features on either side

of the plane containing the null point (i.e., z = –1.8 cm plane), henceforth called the "*null plane*". The exit plane of the PSS is at z = 0 cm. Further, beyond the null plane, one observes that the field lines are converging towards the axis of the ring magnet (i.e., r = 0 cm) with the on-axis magnetic field strength being at its peak at the z = 2 cm. Thereafter, for z > 2 cm planes, the field lines are seen to diverge away from the magnet axis. On the other hand, the situation is completely different for the volume enclosed between the quartz plate (z = –11.8 cm) and the *null plane* (i.e., in the region –11.8 cm < z < –1.8 cm planes). Herein, the magnetic streamlines from z = –11.8 cm to about z = –3.5 cm are almost parallel to the axis of the ring magnet. Thereafter, these magnetic field lines are observed to curve away Fig 2(b), such that they tend to become almost radial, just near the null plane, at the PSS boundary (r = 4.5 cm). The electron cyclotron resonance (ECR) surface is also present in the form of a bowl-shaped contour surface within this region. More details are available in Refs [5-9]. A unique feature that this magnetic field profile provides within the PSS region is a mirror-like configuration across the ECR zone very near to the axis which allows the resonating electrons to undertake multiple transits across the ECR surface. Each time an electron crosses resonance zone it absorbs energy from the microwave via the ECR mechanism enabling it to increase its thermal kinetic energy ($T_{e\perp}$) manifold. Due to the mirror configuration, the microwave power is absorbed by the electrons quite effectively (almost 100%) and thereafter through collisional momentum transfer by plasma, thereby enhancing the power coupling efficiency of the source.

In this study, experimental plasma parameters as well as the plasma simulation results, using COMSOL Multiphysics, obtained by having the CEPS mounted onto a Small Volume Plasma System (SVPS) are presented. The SVPS is a cylindrical stainless-steel chamber 15 cm and 35 cm long. All the experiments conducted in this study have been performed at a base pressure of 6×10^{-6} Torr, obtained using a dual-stage rotary pump (DS 402) and a turbomolecular pump (TV 301 NAV).

Two Langmuir probes (LP) were used to characterize plasma in this set of experiments. One of the LPs was mounted from a side port located 9 cm away from the source mouth (z = 0) to scan in the radial direction of the SVPS expansion chamber. The other LP had an L-shaped shaft that was mounted onto one end (z = 35 cm) of the expansion chamber, i. e. the opposite end to where the PSS is mounted (Fig 1b). The construction of the L probe is given in Fig 3. This probe can be scanned in both radial and axial directions. Both the probes have a cylindrical collection area, measuring 0.25mm in diameter and 4mm in length. Thus the axial and radial profiles of the plasma parameters such as electron density (n_e), electron temperature (T_e) and plasma potential (V_p) can be obtained using these LP. The LP measurements and analysis are presented in the Section 4 below.

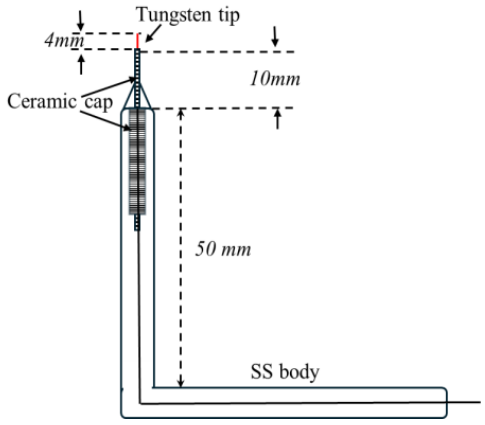

Fig 3. Schematic of the L probe.

3 COMSOL multiphysics simulation

COMSOL is a computational simulation tool which employs the finite element method to resolve various partial differential equations numerically [10-12]. This approach enables the analysis of complex multi-physics phenomena across multiple disciplines. The COMSOL platform [12] offers modular functionality which allows for the integration of multiple components. COMSOL offers the user to undertake simulations in either one-dimensional (1D) or two-dimensional (2D) or 2D-axisymmetric or three-dimensional (3D) geometry; the specific choice being based on the specific requirements of each problem under consideration.

3.1 Description of the model

A two-dimensional drift-diffusion fluid model implemented in COMSOL is employed to simulate Electron Cyclotron Resonance plasma conditions [12]. The objective of the study is to understand the impact of the operating conditions - specifically working pressure and the input microwave power on the plasma properties like electron density (n_e), electron temperature (T_e) and plasma potential (V_p).

To model the electron behavior, COMSOL employs a set of equations that includes the continuity equation, and the electron mean energy equation. These equations are solved simultaneously, while utilizing the drift-diffusion approximation to simplify the momentum equation.

The momentum equations are given as,

$$\frac{\partial n_e}{\partial t} + \nabla . \Gamma_e = R_e - (u.\nabla) n_e \tag{1a}$$

$$\frac{\partial n_\varepsilon}{\partial t} + \nabla . \Gamma_\varepsilon + E . \Gamma_e = S_{en} - (u.\nabla) n_\varepsilon + \frac{Q + Q_{\vartheta en}}{q} \tag{1b}$$

where, R_e is the electron source term. All the terms with suffix e represent parameters of electron species and ε represents corresponding energy values. Other terms represented in the above equations include electron density (n_e), average velocity (u), mean electron energy (n_ε), diffusivity (D), flux (Γ_e) and mobility (μ) terms. Collisional power loss S_{en} represents the energy loss due to elastic and inelastic collisions. Q and $Q_{\vartheta en}$ represent the external heat source and the generalized heat source in plasma module, respectively.

Plasma potential (V_p) is calculated using the Poisson equation.

$$-\varepsilon_0 \varepsilon_r \nabla V_p = \rho \tag{2}$$

where ε_0 and ε_r are the absolute and relative permittivity, respectively and ρ is the space charge density.

Electron flux can be calculated using the following relation,

$$\Gamma_e = -(\mu_e \cdot E)\, n_e - D_e . \nabla n_e \tag{3}$$

Diffusivity terms are given as,

$$D_e = \mu_e T_e \; ; \; D_\varepsilon = \mu_\varepsilon T_e$$

To solve the partial differential equations (1a) and (1b), a set of boundary conditions are used. The primary loss mechanism involves electron-wall collisions, driven by their high thermal speeds and random motion. The model assumes that there is no thermal electron emission and electron reflection from the wall.

$$n.\Gamma_e = \left[\frac{1}{2} v_{eth}\, n_e\right] - \sum_p \gamma_j (\Gamma_j . n) \; ; \; n.\, \Gamma_\varepsilon = \left[\frac{5}{6} v_{eth}\, n_\varepsilon\right] - \sum_p \gamma_j\, \varepsilon_j\, (\Gamma_j . n) \tag{4}$$

γ_j and Γ_j are the coefficient of secondary electron emission and the secondary electron flux, respectively. v_{eth} is the electron thermal velocity and ε_j is the average energy of secondary electrons. The walls of the expansion chamber are electrically grounded. Further, one assumes that both the ion and neutral species are considered to be lost at the wall due to the surface reactions shown in Table 1.

3.2 Chemical reactions in the model

In laboratory systems, plasma generation occurs through the breakdown of gases by the application of any form of external energy. This process involves breakdown of neutral gas into ionized as well as excited states resulting in the formation of plasma. In this study, both surface reactions and the volumetric reactions are incorporated to understand the overall dynamics and characteristics of plasma system (Table 1).

Table 1 Reactions modelled. Ar- Neutral Argon atom, Ar^+ - Argon Ion, Ar^s- Excited Argon atom

Volumetric reaction	
Elastic collision	$e + Ar \Rightarrow e + Ar$
Excitation	$e + Ar \Rightarrow e + Ar^s$
Ionization	$e + Ar \Rightarrow 2e + Ar^+$
Ionization	$e + Ar^s \Rightarrow 2e + Ar^+$
Super elastic collision	$e + Ar^s \Rightarrow e + Ar$
Penning ionization	$Ar^s + Ar^s \Rightarrow e + Ar + Ar^+$
Metastable quenching	$Ar^s + Ar \Rightarrow Ar + Ar$
Surface reactions	
Sticking coefficient = 1	$Ar^+ \Rightarrow Ar$
Sticking coefficient = 1	$Ar^s \Rightarrow Ar$

4 Result and Discussion

In this section, one will discuss both the experimental as well as simulation results. As mentioned in the previous section, both the axial and radial probes were used in the study. The radial probe was 9 cm away from the source mouth, enabling measurements across the diameter of the chamber. The axial probe has an L-shaped probe shaft that can measure in both azimuthal and linear directions along the axis. Due to the damage caused to the probe by the harsh plasma conditions near to the source exit, the axial probe could not undertake measurements close to the source mouth. Hence, for lower working pressures ($p_{fill} \leq$ 1 mTorr), measurements could not be carried out for z < 3 cm. In contrast, at higher pressures ($p_{fill} \geq 5$ mTorr), the probe tip measurements were limited to only z ≥ 7 cm.

4.1 Experimental Results

Figure 4 shows the axial profiles of bulk electron density (n_e), electron temperature (T_e) and plasma potential (V_p) for the discharge generated for an input microwave power of 300 W and Argon filling gas pressure (p_{fill}) of 0.5, 1 and 5 mTorr. As mentioned above, to prevent damage to the probe tip, the axial measurements, presented in this article, are carried out for $z \geq 3$ cm at low pressures ($p_{fill} = 0.5$ and 1 mTorr) and $z \geq 9$ cm at $p_{fill} = 5$ mTorr.

As identified in earlier works [6,9], this damage results from strong ion beams emanating from within the PSS and striking the probe tip. Hence, as the probe tip nears the source exit, one observes the probe top to be glowing. Hence, measurements made at these locations tend to become unreliable. In this set of experiments at a filling pressure of 5 mTorr, one observed this for axial locations < 9 cm, and hence these measurements were not considered in this article. For all three filling pressures presented in this work, one observes the plasma density to peak near to the source and thereafter showing a gradual drop in density as one move away from the source.

In Fig 5, electron density drops from $n_e(z = 3\text{ cm}) \approx 1.6\times10^{12}$ cm^{-3} to $n_e(z = 13\text{ cm}) \approx 0.57\times10^{12}$ cm^{-3} for $p_{fill} = 0.5$ mTorr, $n_e(z = 3\text{ cm}) \approx 1.78\times10^{12}$ cm^{-3} to $n_e(z = 13\text{ cm}) \approx 0.7\times10^{12}$ cm^{-3} for $p_{fill} = 1$ mTorr

and n_e (z = 9 cm) ≈ 3.14×10^{12} cm^{-3} to n_e (z = 15 cm) ≈ 1.965×10^{12} cm^{-3} for p_{fill} = 5 mTorr. This fall in density is expected due to the expanding plasma from the PSS. Electron temperature (T_e) remains almost constant within the expansion chamber viz., T_e ≈ 3 eV for 0.5 mTorr, T_e ≈ 3 eV and 1 mTorr, T_e ≈ 1.8 eV for 5 mTorr, whereas the plasma potential (V_p) drops by about 4 Volts from z = 3 cm to z = 13 cm, with V_p (z = 3 cm) ≈ 18V for 0.5 mTorr, V_p (z = 3 cm) ≈ 20 V for 1 mTorr and V_p (z = 9 cm) ≈ 15 V for 5 mTorr. The elevated plasma potential near the source mouth is attributed to the highly energetic electrons that escape the source region and enter the expansion region, following the magnetic field lines. This results in the development of an ambipolar field that is strong enough to accelerate ions across the source mouth [7]. The L-probe was also used to measure the radial variation of the plasma parameters.

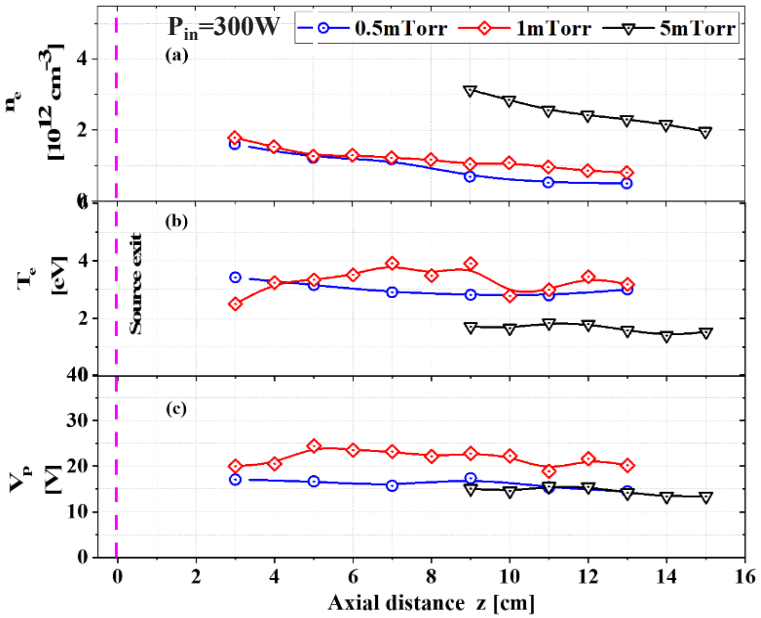

Fig 4. Axial variations of plasma parameters (a) plasma density, n_e (×10^{12} cm^{-3}), (b) electron temperature T_e (eV) and plasma potential Vp (V), measured at 300 W microwave power and filling pressures, p_{fill} = 0.5mTorr (blue solid line, dotted circle), 1mTorr (red solid line, dotted diamond) and 5mTorr (black solid line, dotted inverted triangle).

Figure 6 shows a typical radial profile of the various plasma parameters obtained at z = 9 cm by rotating the axial L probe about its shaft axis. Each rotated angle can be correlated with a radial location. The results presented here are for similar operating conditions at which the axial profiles were taken (Fig 4). From the figure, one observes that the radial profiles of the plasma density peaks on the axis (r = 0 cm) and decays towards the radial edge, (i.e. n_e (r = 0 cm) ≈ 1×10^{12} cm^{-3} to n_e (r = ± 5 cm) ≈ 0.3×10^{12} cm^{-3} for p_{fill} = 0.5 mTorr, n_e (r = 0 cm) ≈ 1.1× 10^{12} cm^{-3} to n_e (r = ± 5 cm) ≈ 0.35×10^{12} cm^{-3} for p_{fill} = 1 mTorr) and n_e(r = 0 cm) ≈ 3×10^{12}cm^{-3} to n_e(r = ± 5 cm) ≈ 0.7×10^{12} cm^{-3} for p_{fill} = 5 mTorr). This implies that the radial density gradient is stronger at higher p_{fill}. = 5mTorr. The radial probe mounted at z = 9 cm, was also used to measure the radial variation of the plasma parameters, as shown in Fig 7. One observes an on-axis peak in plasma density, similar to that observed with the L-probe, (i.e. n_e(r = 0 cm) ≈ 1×10^{12} cm^{-3} to n_e(r = ± 6 cm) ≈ 0.3×10^{12} cm^{-3} for p_{fill} = 0.5 mTorr, n_e (r = 0 cm) ≈ 1.3× 10^{12} cm^{-3} to n_e (r = ± 6 cm) ≈ 0.35×10^{12} cm^{-3} for p_{fill} = 1 mTorr). The electron temperature and plasma potential are observed to remain almost constant radially.

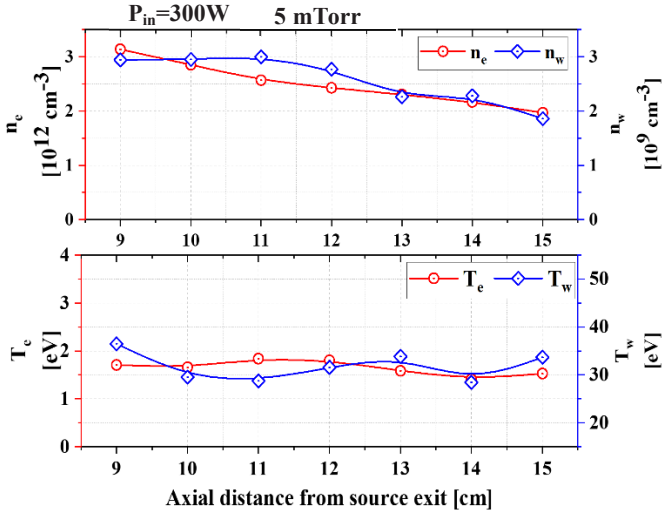

Fig 5. Axial variation of (a) density n_e ($\times 10^{12}$ cm^{-3}), n_w ($\times 10^{12}$ cm^{-3}) (b) temperature T_e (eV) and T_w (eV) for both bulk (e) and warm (w) electrons. Data taken at 5 mTorr pressure and 300 W microwave power. Bulk and warm parameters are represented by red solid line, dotted circle and blue solid line, dotted diamond, respectively.

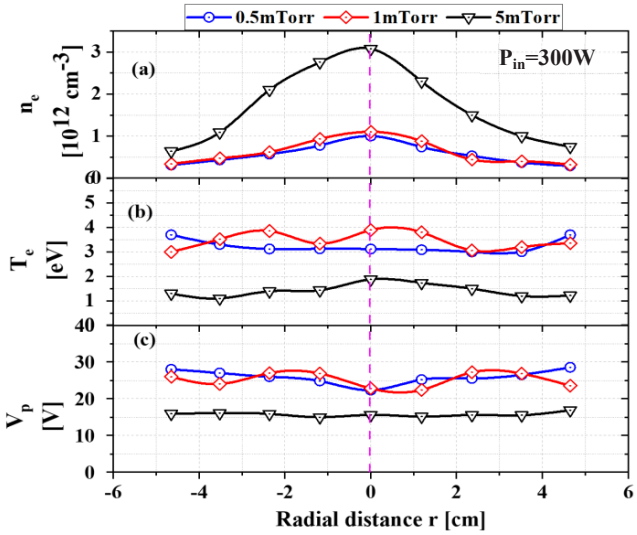

Fig 6. Radial variation of plasma parameters (a) Plasma density n_e ($\times 10^{12}$ cm^{-3}), (b) electron temperature T_e (eV) and (c) plasma potential Vp (V) measured by rotating the axial L probe about its shaft axis. The plasma parameters at 300 W microwave input power and operating gas pressures, p_{fill} = 0.5 mTorr (blue solid line, dotted circle), 1mTorr (red solid line, dotted diamond) and 5mTorr (black solid line, dotted inverted triangle) are shown in the figure.

4.2 Simulation Results

COMSOL simulation is performed to understand the plasma characteristics at diferent input powers at 5mTorr pressure. One could not carry out simulations for pressures below 5 mTorr due to steady-state convergence issues, as most low-pressure plasma models provided in the COMSOL user manual are applicable only to higher pressures (20 mTorr to 1 Torr) [12-14]. It is worth noting that the experimental

system has 2D- axisymmetric geometry. Hence, one would prefer to undertake plasma simulations using this geometry. However, one observed that plasma simulations were completely different from the experimental results, with the plasma being formed far away from the ECR zone, which does not align with the physical interpretations. The reasons for this are being investigated. However, plasma simulations carried out using the 2D geometry provided results that are relatively close to the experimental results and are presented here to provide some initial understanding of the plasma dynamics. Plasma parameters were computed within the CEPS and the expansion chamber, imposing the boundary conditions mentioned in section 3. It is assumed that all particles incident on the wall are absorbed (with a sticking coefficient of 1) and there is no thermionic emission (the thermionic emission coefficient is zero).

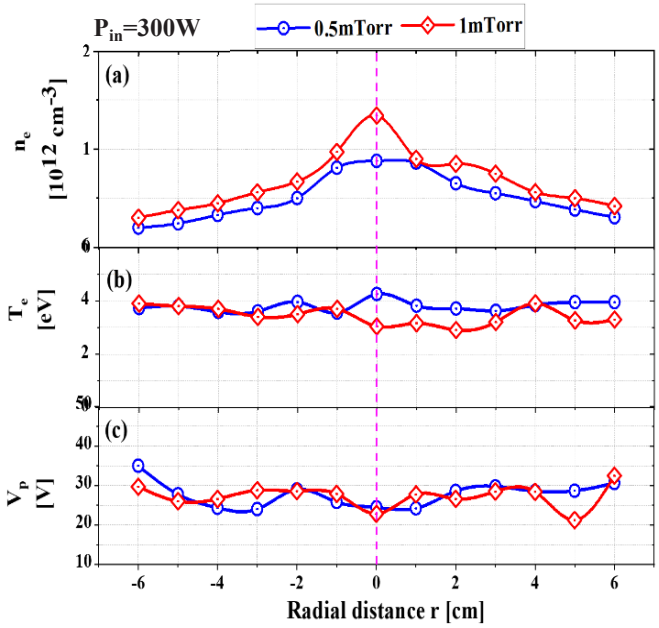

Fig 7. Radial variation of plasma parameters (a) Plasma density n_e ($\times 10^{12}$ cm^{-3}), (b) electron temperature T_e (eV) and (c) plasma potential V_p (V) measured by radial probe. The plasma parameters at 300 W microwave input power and operating gas pressures, p_{fill} = 0.5 mTorr (blue solid line, dotted circle) and 1mTorr (red solid line, dotted diamond) are shown in the figure.

The key factor for any ECR plasma is the resonant transfer of the electromagnetic energy to the particle energy of resonating electrons. Thus the resonance field (Bresonance) is very important for power transfer and is solely dependent on the microwave frequency (ω), given by the relation, $B_{resonance}$= (ωm_e)/q. The resonance magnetic field, corresponding to the 2.45 GHz microwave frequency used in the experiments presented here, is approximately 875 G. The experimental system presented here has different distinct regions with completely different magnetic profiles. The fundamental property of ECR plasmas is the transfer of electromagnetic energy to particle energy in and around the ECR zone, which is located within the PSS for this set of experiments. This zone is the source of plasma generation, and the simulations need to be carefully modelled in this region. Thereafter, one has the null plane just inside the PSS. The region surrounding the null plane has strong magnetic field gradients, which would imply complex plasma dynamics in its vicinity. Thereafter, once the plasma flows out of the PSS and the null plane zone, one expects a more benign region of plasma expansion along the diverging magnetic fields. Hence, to reduce computational errors, a functional mesh adaptation is given for the 875G resonance zone. This is ideal for complex models like ECR plasma, so that the 875G region is appropriately meshed (Fig 8) for the plasma model to ensure

that the errors are less [14]. The magnetic streamline structure of the SVPS is presented in Fig 9. Steady state simulation results for 300W input power at 5 mTorr pressure are shown in Fig 10. The microwave is launched through the quartz window and the microwave power is found to be absorbed within the ECR zone, which is also responsible for the formation of dense plasma within the expansion chamber. Figure 10(a), indicates that the power is deposited in the resonance layer (875G contour), which also corroborates with experimental observations. Subsequently, one expects that the resonating electrons which have absorbed microwave energy as it transits through the resonance layer, to undergo electron-neutral impact ionization processes and trigger plasma generation within the PSS. The lighter and energetic electrons, formed within the PSS, being more mobile than the heavier ions will tend to leave the PSS faster following the magnetic field lines and ultimately flow into the expansion chamber. This creates an ambipolar field across the source mouth which allows the sluggish ions to accelerate out of the PSS resulting in a quasi-neutral plasma filling up the expansion chamber.

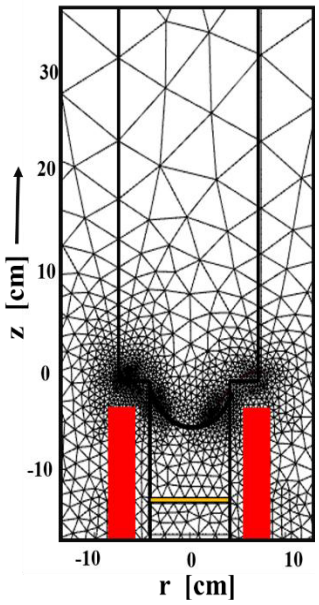

Fig 8. Adaptation mesh.

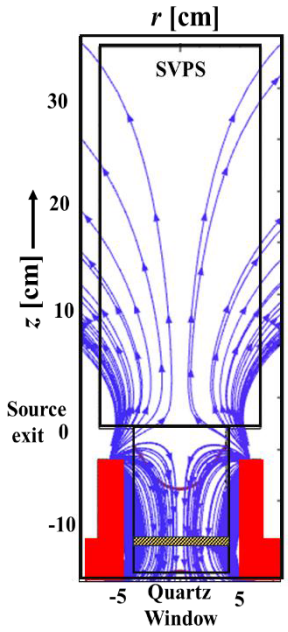

Fig 9. Streamline and contour.

The on-axis electron temperature (T_e) profile (Fig 10c) shows that the source mouth exit is relatively hotter than the expansion chamber. Now the plasma potential (Vp), with respect to the floating potential (V_f), is linearly proportional to the electron temperature. Hence this transition from a hotter T_e to a cooler T_e is also indicative of the existence of an ambipolar field across the source mouth. This ambipolar field would be ideal for the ion beams to accelerate out of the PSS into the expansion chamber, as explained earlier. The constriction of the magnetic field lines towards the axis (Fig 9) at $z - z_0 = 4 - 5$ cm, after the null plane (z_0) aids in an enhancement of electron density as is evident from the surface plots of Fig 10(b). It is to be noted here that the 2D geometry results have shifted the magnetic profile by about 1.8 cm towards the expansion chamber. This has also resulted in the null plane and the subsequent constriction to shift by a similar distance. Hence, the null plane is at $z_0 = 0$ in the simulations as against $z_0 = -1.8$ cm in the experimental setup. Beyond this axial distance from the source mouth, the on-axis plasma density is observed to decrease. This can be attributed to the expanding magnetic field lines which allow for the plasma to also expand and fill up the plasma volume. Figure 10(b) corroborates this inference since the radial

profile becomes almost constant beyond $z - z_0 \approx 20$ cm. It is also observed that the electron temperature decreases along the expansion chamber with an initial parabolic profile close to the source mouth, gradually becoming radially constant away from the source mouth. The higher electron temperature of 2.7eV is in the region with highest streamline density near the magnet. Figure 10(d) also shows that the plasma potential is highest near the source exit, around 17V, and gradually decreases with distance from the source mouth, which is indicative of the existence of ion beams, as explained earlier. The plasma density is observed to increase significantly in the simulated results as the input microwave power is increased (Fig 10). However, earlier experimental observations by Ganguli *et al* indicate that the plasma density decreases as the power increases for operating pressures above 5 mTorr [5]. One possible reason for this difference is the idealized assumptions considered in COMSOL simulations that might not fully capture the complex real experimental conditions, especially within the PSS conditions. Another possible reason might be the difference in the electron populations.

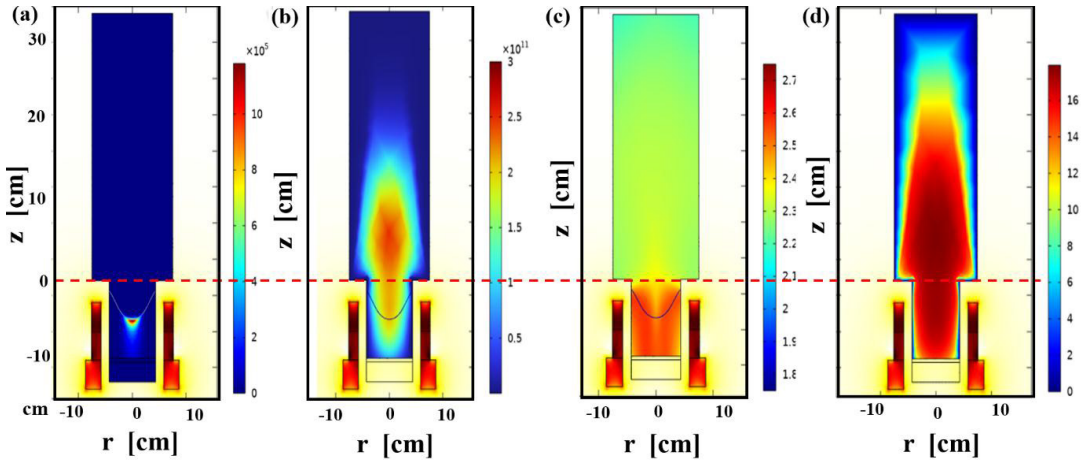

Fig 10. Surface plot of Comsol simulated plasma parameters: (a). Power deposition profile, (b). Electron density, (c). Electron Temperature, (d). Plasma potential.

Figure 11 presents the axial profiles of Plasma density (n_e), Electron Temperature (T_e) and Plasma potential (V_p) at p_{fill} = 5mTorr for input power, P_{in} = 300W, 400W and 500W. One observes that the electron density shows an initial increase till about z – z_0 = 5 - 7 cm, i. e. just near to the maximum constriction of magnetic field lines close to the axis after the null plane. This increase in density is about 8-10% with respect to that observed at source exit (z_0). Thereafter, the density is observed to decrease gradually. Similar observations have been reported in earlier experiments [6], wherein one could scan close to the source mouth. The typical variation of the simulated plasma parameters from z = 9 cm (closest point measured in this set of experiments) and z = 13 cm (the farthest point measured) for 5 mTorr are stated here as follows: *ne* (z = 9 cm) $\approx 0.12\times10^{12}$ cm^{-3} to n_e (z = 13 cm) $\approx 0.1\times10^{12}$ cm^{-3} for P_{in} = 300W, ne (z = 9 cm) $\approx 0.1\ 6\times10^{12}$ cm^{-3} to n_e (z = 13 cm) $\approx 0.13\times10^{12}$ cm^{-3} for p_{in} = 400W and n_e (z = 9 cm) $\approx 0.205\times10^{12}$ cm^{-3} to n_e (z = 13 cm) $\approx$ 0.17×10^{12} cm^{-3} for p_{in} = 500W. This fall in density is expected due to the expanding plasma from the PSS. Electron temperature (T_e) remains almost constant within the expansion chamber viz., $T_e \approx 2.3$ eV, whereas the plasma potential (V_p) drops by about 2V from z = 9 cm to z = 13 cm, with V_p (z = 9 cm) $\approx$ 18 V for 300, 400 and 500W. Figure 12 depicts the comparison between the simulated data and the experimental results for 300W input power and a pressure of 5 mTorr. There is an order of difference in the plasma density between the experiment (10^{12} cm^{-3}) and the simulation results (10^{11} cm^{-3}). This clearly shows that the trends in the variation of the plasma parameters between the simulated and experimental results match quite closely.

However, the mismatch in absolute values can possibly be attributed to the following reasons. The COMSOL simulated model is a single electron population model, whereas the experimental results have identified the existence of two electron populations, bulk (~1-2 eV) and warm (~30-50 eV) [5-6] as shown in Fig 4.

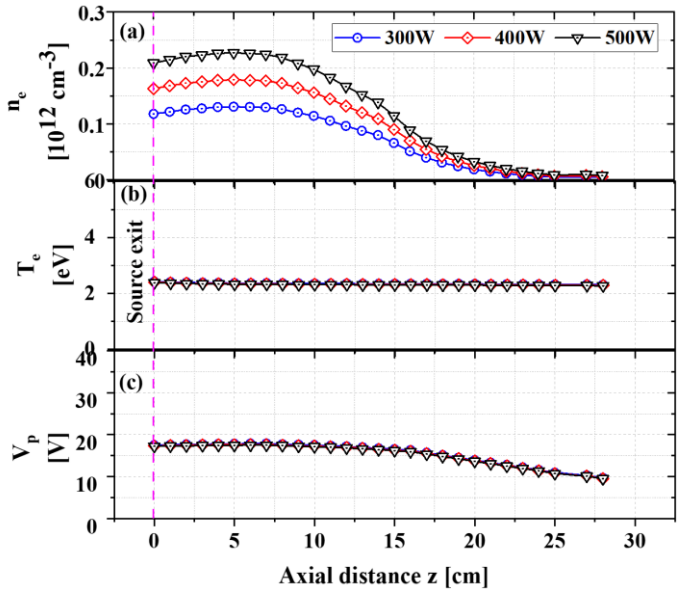

Fig 11. Axial plasma parameters measured at 5 mTorr gas filling pressure and microwave input powers of 300 W (Blue solid line, dotted circle), 400 W (Red solid line, Dotted diamond) and 500 W (Black solid line, Dotted down triangle) for (a) electron density, n_e (10^{12} cm^{-3}), (b) electron temperature, T_e (eV) and (c) plasma potential, V_p (V).

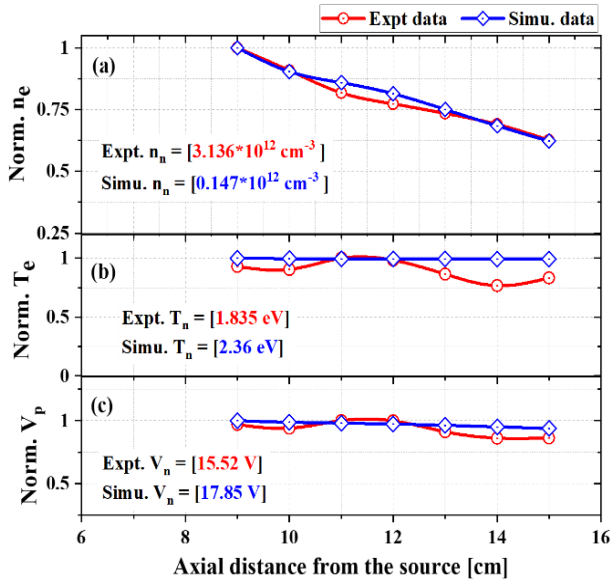

Fig 12. Normalized plasma parameters at 5 mTorr, 300W comparison with experimental data (Red solid line, dotted circle) and simulated data (Blue solid line, Dotted diamond) shown for (a) electron density, n_e, (b) electron temperature, T_e and (c) plasma potential, Vp. Normalization factor n_n = max (n_e), T_n = max(T_e) and V_n = max (V_p) of each data set.

This warm population, observed in the experiments, is not accounted for in the simulations. This could potentially explain the difference between experimental and simulation results in the output parameters. This disparity in absolute values may be attributed to the various simplifications of the model considered while using COMSOL. This was, primarily, due to the limited computational resources available in the lab. Some of these simplifications are highlighted below. One issue is the use of 2D geometry when, for all practical purposes, a 2D-axisymmetric geometry would have been appropriate for this experimental system. However, the plasma simulations are unable to model microwave absorption at the ECR zone, which is crucial for ECR plasma production. This needs to be resolved first to use the same and is now being investigated in the lab. On the other hand, the 2D geometry simulations at least resulted in maximum absorption of microwave power around the ECR zone, which at least provided some semblance to use these results. A 3D geometry simulation would have been most appropriate, but it was not possible due to the limited resource availability in the lab. Apart from these logistical issues, one can also identify scientific considerations for the mismatch in absolute values. It may be noted that the COMSOL simulation models assume a single electron population model, whereas the experimental results have clearly identified the existence of two electron populations, bulk (~1-2 eV) and warm (~30-50 eV) [5-6] as shown in Fig 5. This warm population has been observed regularly in experiments [6-9]. They have been identified to play a significant role in sustaining the discharges within the expansion chamber, especially at higher pressures [7-8]. This could also potentially explain the differences between the absolute values of the plasma parameters in the experimental and simulation results, even though the trends in the profile variation are identical. Another important issue is the null point just in front of the source mouth, which could appropriately be simulated using 2D-axisymmetric or 3D geometry, the latter being more accurate but also quite computationally intensive. Thus, in future works, one will explore the possibility of identifying the issues with the 2D-axisymmetric model or work towards the 3D geometry simulations to explain the observations more accurately to identify the exact physics involved in the process. The above discussion using 2D-geometry can still be considered valid since the difference in simulations based on the geometry used would have more prominent effects within the source region and near the null point, wherein the magnetic field profiles are highly complex, whereas the region within the expansion chamber has a simple diverging magnetic field. Despite the aforementioned issues, one can still consider the results to have similar trends, as they have been compared for $z \geq 9$ cm, between the experimental and simulation results.

5 Summary

The experiments were conducted at the operating pressures of 0.5mTorr, 1mTorr and 5mTorr, while the plasma simulation was done at 5mTorr. One did not simulate for pressures below 5mTorr since the steady-state simulations in the software did not consistently converge, suggesting that the current model may not be appropriate for these lower pressure regimes. LP data for various pressures were analyzed to get an insight into the variation of plasma properties within the expansion chamber. Another significant point to be noted is that the experiments indicated the presence of strong ion beam accelerated out of the source exit attributed to the more energetic and lighter electrons emanating faster than the ions from the source region and through source mouth and across the complex fields around the null point into the expansion chamber. Thereafter, following the expanding magnetic field lines. This would result in the development of a negative potential drop across the source mouth, which aids in accelerating the ion beam out of the source. Additionally, in the COMSOL simulation, plasma parameters were investigated for varying the microwave power. Although the absolute value of the density and electron temperature differ from the experimental results, the normalized density profile shows a similar profile. Plasma potential and electron temperature are also found to follow a similar profile. The variation in the absolute values can be explained by the fact that real plasma behaviour includes complex physics and additional electron loss mechanisms, which are not accounted for in the current COMSOL model used in the simulation. However, since both exhibit a similar pattern, it can be concluded

that this work demonstrates a strong agreement between the simulation and experimental results, offering valuable insights into the plasma behaviour inside the expansion chamber.

Acknowledgments

One of the authors (DS) acknowledges the financial support from DST SERB project (ECR/2017/000993) for the support to work on this ECR Plasma system. The author (NB) would like to extend gratitude to AICTE for the scholarship received through the QIP program.

References

1. Bathgate S N, Bilek M M M, Mckenzie D R, Electrodeless plasma thrusters for spacecraft: a review, *Plasma Sci Technol*, 19(2017) 083001; doi.org/10.1088/2058-6272/aa71fe.
2. Mazouffre S, Electric propulsion for satellites and spacecraft: established technologies and novel approaches, *Plasma Sources Sci Technol*, 25(2016)033002; doi.org/10.1088/0963-0252/25/3/033002.
3. Garrigues L, Coche P, Electric propulsion: comparisons between different concepts, *Plasma Phys Control Fusion,* 53(2011)124011; doi.org/10.1088/0741-3335/53/12/124011.
4. Ganguli A, Akhtar M K, Tarey R D, Absorption of high-frequency guided waves in a plasma-loaded waveguide, *Phys Plasmas*, 14(2007)102107; doi.org/10.1063/1.2799161.
5. Ganguli A, Tarey R D, Permanent magnet compact electron cyclotron resonance plasma generator, Indian Patent #301583Patentee: IIT Delhi, 2006.
6. Ganguli A, Tarey R D, Narayanan R, Verma A, Sahu D and Arora N, A Compact ECR Plasma Source Developed at IIT Delhi – Physics and Applications, *Asian J Phys*, 30(2021)119–135
7. Ganguli A, Tarey R D, Arora N, Narayanan R Development and studies on a compact electron cyclotron resonance plasma source, *Plasma Sources Sci Technol*, 25(2016)025026; doi.org/10.1088/0963-0252/25/2/025026.
8. Ganguli A, Tarey R D, Narayanan R, Verma A, Evaluation of compact ECR plasma source for thruster applications, *Plasma Sources Sci Technol*, 28 (2019)035014; doi.org/10.1088/1361-6595/ab0969.
9. Verma A, Ganguli A, Sahu D, Narayanan R, Tarey R D, Thrust evaluation of compact ECR plasma source using 2-zone global model and plasma measurements, *Plasma Sources Sci Technol*, 29(2020)085007; doi.org/10.1088/1361-6595/ab97a5.
10. Lieberman M A, Lichtenberg A J, Principles of plasma discharges and material processing, 2nd Edn (Wiley, New York).
11. Ganguli A, Tarey R D, Understanding plasma sources, *Curr Sci*, 83(2002)279–290.
12. COMSOL Application Library Manual, Plasma Module version 6.1.
13. COMSOL plasma module user guide.
14. COMSOL dipolar microwave plasma source user manual.
15. Pelletier J, Distributed ECR Plasma Sources, High Density Plasma Sources, (1994)380–425; doi.org/10.1016/B978-081551377-3.50010-4.
16. Jarrige J, Elias P, Cannat F, Packan D, Performance Comparison of an ECR Plasma Thruster using Argon and Xenon as Propellant Gas, IEPC-2013-420.
17. Correyero S, Ahedo E, Jarrige J, Packan D, Plasma beam characterization along the magnetic nozzle of an ECR thruster, *Plasma Sources Sci Technol*, 28(2019)095004; doi. 10.1088/1361-6595/ab38e1.

[*Received*: 24.01.2025; *Rev recd*: 25.02.2025; *accepted*: 26.02.2025]